RSC Advances




ROYAL SOCIETY OF CHEMISTRY

www.rsc.org/advances

**Table of Contents**

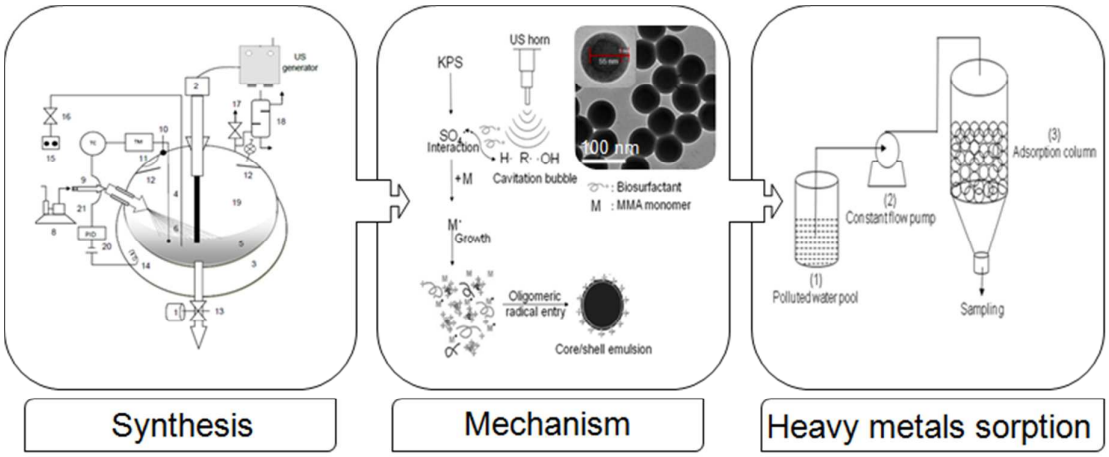


Non-toxic core/shell poly(methyl methacrylate)/surfactin nanoparticles was synthesized via US route for removal of $Pb^{2+}$, $Cd^{2+}$, $Cu^{2+}$ and $Fe^{2+}$ ions

# Sonochemical synthesis of poly(methyl methacrylate) core/surfactin shell nanoparticles for recyclable removal of heavy metal ions and its cytotoxicity

Debasree Kundu[a,‡], Chinmay Hazra[a,‡], Aniruddha Chatterjee[b,*], Ambalal Chaudhari[a] and Satyendra Mishra[b]

[a]*School of Life Sciences, North Maharashtra University, Jalgaon, Maharashtra, India*

[b]*University Institute of Chemical Technology, North Maharashtra University, Jalgaon, Maharashtra, India*

*Corresponding author. Tel.: +91 257 2258420. Fax: +91 257 2258403. E-mail: aniruddha_chatterjee2006@yahoo.co.in

[‡]These authors contributed equally as first authors in this manuscript

## Abstract

This work deals with the use of intensified processes based on the combined use of acoustic cavitation and biosurfactant for enhancing the latex yield and colloid characteristics in the acoustic atomized microemulsion polymerization of methyl methacrylate (MMA). It was compared with oil/water (o/w) modified atomized microemulsion process in a conventional mechanically agitated reactor. The synthesized nanoparticles were further applied for selective removal of $Pb^{2+}$, $Cd^{2+}$, $Cu^{2+}$ and $Fe^{2+}$ ions from water. Batch adsorption equilibrium was reached in 30 min and maximum uptakes for $Pb^{2+}$, $Cd^{2+}$, $Cu^{2+}$ and $Fe^{2+}$ in non-competitive adsorption mode were 86, 52, 80, and 71 mg $g^{-1}$, respectively at 30 $^{o}$C. Adsorption data were fitted well to Langmuir isotherm and pseudo-second-order models for kinetic study. The heavy metals loaded on these nanoparticles could be desorbed in acid or EDTA solution and adsorption capacity of the regenerated adsorbent was not significantly declined after five cycles of adsorption-desorption cycles. Negative values of Gibb's free energy change ($\Delta G^{o}$) showed that the adsorption was feasible and spontaneous and negative values of enthalpy change ($\Delta H^{o}$) confirmed exothermic adsorption. A cell viability study indicated that the nanoparticle is non-cytotoxic in nature. Lastly, a continuous filtering-type water purification device was designed and constructed to successfully attain the World Health Organization standard for drinking water.


**Keywords:** Core-shell nanoparticles; Poly(methyl methacrylate); Ultrasound; Adsorption; Heavy metals

## 1. Introduction

The discharge of heavy metal wastes into the effluent over the past few decades has inevitably resulted in an increased flux of metallic substances into the global aquatic environment due to their acute toxicity, non-biodegradability, and build-up in high concentrations.[1-7] Point and non-point source industrial runoffs from battery manufacturing, printing and pigment, tanneries, oil refining, mining smelting, electroplating, paintings, and most recently e-wastes resulted in elevated levels and chronic toxicity of lead ($Pb^{2+}$), cadmium ($Cd^{2+}$), copper ($Cu^{2+}$) and iron ($Fe^{2+}$).[8,9] Consequently, the maximum permissible limit of these heavy metal ions in inland surface water and drinking water are 0.006, 0.01, 0.25, and 0.1 mg $l^{-1}$, respectively, according to US EPA.

Due to the inherent advantages of adsorption technology, it is the most widely studied because of its low operational and maintenance costs and high efficiency, especially for the heavy metal ions with low concentration.[10,11] A large number of polymers incorporating a variety of chelating-ligands (e.g., poly(ethyleneimine), iminodiacetate, amidoxime, phosphoric acid, dithiocarbamate, thiazolidine, $Fe_3O_4$) have been prepared and their adsorption and analytical properties investigated.[12-14] As reported in these studies, the carboxyl and amine groups have been found to be two most effective functional groups for heavy metal removing from aqueous solutions.[12,14] The idea of using different amino acid based chelating ligands stems from (i) higher reactivity of these chelating ligands with metal ions; (ii) higher structural flexibility and durability of these ligands; (iii) easy modification by existing chemical methods to facilitate desorption under mild conditions; and (iv) lower material and manufacturing costs.[12] In spite of a huge amount of research effort being devoted towards natural and synthetic polymers, most commercial adsorbents are micron sized and highly porous beads to ensure adequate surface area for adsorption of different substances including metal ions and proteins.[13] On the other hand, for nanoscale materials,

even though they aggregate into microspheres, it is still difficult to recycle them for their superior dispersive properties in solution. Moreover, conventional separation methods, including centrifugation or filtration, are time consuming and may lead to loss of the adsorbent. Hence, it is essential to develop new greener and ecologically benign polymeric adsorbents to offset the disadvantages of non-selective adsorption, biocompatibility, operational costs for absorbent separation and recycling, and most importantly low specific surface area as well as low internal diffusion limitation. Taking into cognizance of these shortcomings, there is an upswing in the publications which deals with encapsulation of nanoparticles with different organic shells in most recent literature.[13,14] However, the preparation and encapsulation of these nanoparticles are generally two or more separate processes.[5,13,14] Most importantly, heavy metal ion adsorption experiments are often performed in a batch-by-batch manner, a method which is impracticable in drinking-water treatment. Thus, the utilization of a continuous metal ion adsorption filter system device is highly desirable for the purification of drinking water. However, such a technique for efficient and fast purification of drinking water by removing low concentration heavy metal ion pollutants has rarely been reported. Further, the non-cytotoxicity of the materials is also another vital factor for a material to be a novel and useful adsorbent with simultaneous heavy metals sorption. Unfortunately, as far as we can ascertain, there are no literature reports on the toxicity level.

Considering the biocompatibility, low toxicity and high adsorption ability of both poly(methyl methacrylate) (PMMA) and surfactin, here we report preparation and characterization of PMMA-surfactin core/shell nanoparticles. PMMA was chosen to be the polymeric core in this study for a couple of reasons. Firstly, PMMA is non-toxic, cheap and easy to obtain. PMMA exhibits excellent material properties such as exceptional mechanical strength, hardness, high rigidity, transparency, and good insulation properties.[15,16] However,

the hydrophobic surface of PMMA prevents adhesion to other substances, limiting its spectrum of applications. Some efforts have been made recently to incorporate nanoscale zerovalent iron, chitosan, polyethyleneimine *etc.*, into PMMA to obtain multipurpose functional nanoparticles. However, the resulting composite materials still fell short of expectations because of the significant difference in permittivities of the two components and the inhomogeneity between the two phases. These requirements inspired us to design a green one-pot synthesis for synthesizing biosurfactant functionalized core/shell PMMA nanoparticles. Being water soluble, nontoxic and non-immunogenic in nature, the biosurfactant surfactin is frequently used for heavy metal remediation. Other advantages include their production from inexpensive agro-based raw materials and organic wastes and retention of their activity even at extremes of temperature, pH and salt concentration. Introduction of surfactin in a polymer structure offers several biological advantages; *e.g.* it imparts a prolonged lifetime to the polymer in the bloodstream due to decreased uptake of surfactin-conjugates by the reticuloendothelial system of the body. Herein, the feasibility of enhancing the latex yield and colloid characteristics through the use of intensified processing technique, *i.e.* ultrasound (US) assisted atomized microemulsion polymerization is reported here and compared with a recently developed method from our group[17-23] that makes use of an oil/water (o/w) modified atomized microemulsion process (henceforth named as conventional atomized microemulsion) to synthesize polymer-biosurfactant core/shell nanoparticles for heavy metals remediation. Despite the intensive investigation on US polymerization of MMA,[16,24-28] to the best of our knowledge, there are no reports highlighting (i) core/shell morphology, specially using surfactant of microbial origin; (ii) minimal use of surfactant to achieve high PMMA solid content (traditional and US polymerization uses up to 20 and 2 wt.% of surfactant of the total reactor charge, respectively[29,16]); and (iii) the process intensification characteristics. Next, we investigated the adsorption capacity of the

nanoparticles for $Pb^{2+}$, $Cd^{2+}$, $Cu^{2+}$ and $Fe^{2+}$ heavy metal ions in different pH solution and metal ion uptake capacity as a function of contact time, metal ion concentration and adsorbent dosage. We also studied the adsorption isotherms, kinetics and thermodynamics to understand the mechanism of the adsorption process and explored the effect of the background electrolytes, desorption and adsorbent reuse. A continuous filtering adsorption device with a rapid and high adsorption performance for different heavy metal ions was designed and built by using as-synthesized nanoparticles as the filtration adsorbents in order to demonstrate a continuous heavy metal ion removal process in drinking water purification.

## 2. Experimental

### 2.1. Chemicals and reagents

$Pb(NO_3)_2$, $CdCl_2.2.5H_2O$, $Cu(NO_3)_2.3H_2O$, $FeCl_3.6H_2O$, ammonium hydroxide, hydrochloric acid, humic acid (HA), methyl methacrylate (MMA, density: 0.94 g $cm^{-3}$ at 25 °C, A.R. grade), n-hexanol and methanol were purchased from S.D. Fine Chemicals Ltd. (Mumbai, India). MMA was used after the removal of inhibitors by a procedure reported by Bhanvase *et al.*[16] Potassium per sulfate (KPS, $K_2S_2O_8$) was procured from Qualigens India Ltd. (Mumbai, India). HA was treated as per Tang *et al.*[30] Double distilled and deionized water (DDIW) was used during polymerization and in other experiments.

### 2.2. Production and purification of surfactin

Surfactin was obtained from the cell free broth of *Bacillus clausii* BS02 following the method described in Liu *et al.*[31] The isolation, purification and structural analysis were done according to Namir *et al.*[32] Purified surfactin consisted of a peptide loop containing seven amino residues bonded to a β-hydroxyl fatty acid chain with 15 carbon atoms (Fig. S1; see

ESI). The physico-chemical characteristics of this biosurfactant are listed in Table S1 (see ESI).

### 2.3. Synthesis of PMMA nanoparticles (nPMMA) using acoustic and conventional atomized microemulsion process

US assisted atomized microemulsion polymerization was carried out for synthesizing nPMMA-surfactin core/shell ($nPMMA_{US}$) particles in a cavitation reactor (Fig. S2a in ESI) using surfactin as biosurfactant (0.5% of MMA) instead of sodium dodecyl sulfate (SDS) and US probe in place of mechanical agitator. The reactor used consists of a jacketed glass vessel provided with US horn equipped with a generator and controlled by standard power source. The specifications of the US horn are as follows: operating frequency, 22 kHz; power rating, 240 W; diameter of stainless steel tip, $1.3 \times 10^{-2}$ m, surface area of US irradiating face, $1.32 \times 10^{-4}$ $m^2$, expected US intensity, $3.4 \times 10^5$ W $m^{-2}$ and the horn was operated at 50% amplitude. The actual power dissipation as measured using calorimetric method was 45.5 W giving an energy transfer efficiency of 18.9%. The depth of the horn in the solution was 1 cm and it was located at the centre of the vessel. The temperature was maintained at 55 $^oC$ (±1) throughout the experimental investigation for 1 h.

For comparison, conventional atomized microemulsion process was used to synthesize nPMMA-surfactin core/shell ($nPMMA_{AM}$) particles in which the temperature of the polymerization reactor was maintained at 55 $^oC$ (±1) for 1 h as shown in Fig. S2(b) (ESI).[23,33] The reactor setup was similar except for the fact that US horn was replaced by mechanical stirring.

The nPMMA particles were isolated by drop wise addition of the latex into methanol with constant stirring, and the mixture was kept overnight for uniform dispersion of

precipitate. The precipitated particles were filtered under vacuum and washed several times with methanol/water (1:1) and then dried in a vacuum desiccator for 48 h at 40 $^{o}$C.

### 2.4. Characterization

Calculations of monomer conversion, solid content, molecular weights and polydispersity index (PDI) are described in Supporting Information (see ESI). A transmission electron microscope (TEM, CM200, Philips) operating at 120 kV was used to image and study the morphology of the samples. The TEM samples were prepared by drop casting samples dispersion in the carbon coated copper (200 mesh) grid. The Z-average particle size, the distribution of the particle size and ζ-potentials of nanoparticle latexes were measured using a Zetasizer (NanoZS, Malvern Instruments Ltd., UK). The diameters of highly diluted dispersions (in $10^{-3}$ M HCl) were measured, at several temperatures between 20 and 50 °C. The ζ-potentials were measured in 1 mM NaCl solution at room temperature. The pH values of nanoparticle dispersions were adjusted to be in a range of 1-12. The isoelectric points were determined at a pH where the ζ-potential is zero. Fourier transforms infrared (FTIR) spectra of the biosurfactant surfactin and nPMMA particles were recorded on FTIR-8000 (Shimadzu, Tokyo, Japan) at resolution of 0.5 $cm^{-1}$ with an average of 32 scans. Quantitative measurement of grafted surfactin ($G_{SR}$%) was done using 2,4,6-trinitrobenzene sulfonic acid (TNBS) assay.[23] $^{1}$H-NMR measurements of $nPMMA_{AM}$ and $nPMMA_{US}$ particles were carried out on a Mercury Plus 300 NMR spectrometer (Varian, USA). The samples were dissolved in $CDCl_3$ as an internal standard for carbon and TMS was used as an internal standard for proton. X-ray photoelectron spectroscopy (XPS) measurements on the $nPMMA_{AM}$ and $nPMMA_{US}$ particles were carried out using a X-ray photoelectron spectrometer (VG Multilab 2000-Thermo Scientific, UK, K-Alpha) with a multi-channel detector, which can endure high photonic energies from 0.1 to 3 keV. Binding energies (BE)

were referred to the C 1s line of adventitious carbon at 284.6 eV and determined with the resolution of ± 0.1 eV. These spectra were fitted assuming Gaussian-Lorentzian distribution for each peak, with a linear background in order to determine the binding energy of the various element core levels.

### 2.5. Batch adsorption experiments

The batch adsorption procedure consisted of distributing 2.00 mg of $nPMMA_{US}$ or $nPMMA_{AM}$ particles and 10 ml water solution containing selected concentrations of $Pb^{2+}$, $Cd^{2+}$, $Cu^{2+}$ and $Fe^{2+}$ in a series of 20 ml glass tubes. All tubes were sealed and shaken in a temperature-controlled shaker incubator set at 120 rpm. Effect of pH on the adsorption was studied in the pH range of 2.0-10.0 and the pH was adjusted using stock $HNO_3$ and NaOH solutions. For studying the effect of organic matter, a certain amount of HA solution was added to each of the tubes. The sorption kinetics was performed at the optimum pH (6.0) using 50 ml of each metal solution of known concentration (5-50 mg $l^{-1}$) with 2.00 mg adsorbent at 30 $^{o}$C. For the isotherm experiments, the initial solution pH was kept at 6.0, with varying metal concentration ranging from 5-50 mg $l^{-1}$ at three different temperatures 30, 40 and 50 $^{o}$C. At appropriate time intervals, solutions were centrifuged, and the supernatant was analysed to obtain residual heavy metals ion concentration. To determine the amount of ions adsorbed onto the surfaces, the difference between the initial and the equilibrium ion concentration by inductively coupled plasma-atomic emission spectrometer (ICP-AES) (Arcos, Spectro, Germany) was measured (±0.01%). The concentrations of the adsorbed ions onto surfaces were determined through a calibration curve for the known ions concentration in the individual aqueous solution. The amount of metal ion sorbed at time $t$ ($q_t$), was calculated from the mass balance equation:

$$q_t = (C_0 - C_t)V/M \quad (1)$$

where, $q_t$ (mg $g^{-1}$) is the amount of heavy metals adsorbed at time $t$, $C_0$ (mg $l^{-1}$) is the initial heavy metals concentration, $C_t$ (mg $l^{-1}$) is heavy metal concentration at time $t$, $V$ (ml) is the volume of heavy metal solution, and $M$ (g) is the adsorbent mass.

Desorption experiments were conducted to assess the reuse and regeneration potential of $nPMMA_{US}$ particles. After the adsorption experiments, the nanoparticles carrying metal ions(s) were separated. The saturated nanoparticles were dispersed into 10 ml of EDTA or HCl solution (0.01 mol $l^{-1}$). After shaking at 120 rpm for 60 min, the nanoparticles in the solid phase were separated from the solutions and the concentration of each metal ion in the supernatant was assayed. The regenerated nanoparticles were washed with DI water three times, and dried for reuse.

### 2.6. Column dynamic study

Continuous-flow experiments were conducted in a glass column (internal diameter of 1.5 cm and a height of 25 cm). The column was packed with $nPMMA_{US}$ particles at a bed height of 2 cm. The device is consisted of three parts: first is the container to hold simulated polluted water, second is the pumping system used to pump polluted water through the continuous filtering device; and third is the filter filled with $nPMMA_{US}$ particles. The synthetic simulatory effluent (aqueous solutions of $Pb^{2+}$, $Cd^{2+}$, $Cu^{2+}$ and $Fe^{2+}$; 30 mg $l^{-1}$) at pH 6.0 was fed upwards into the column using a peristaltic pump at a flow rate of 1 ml $min^{-1}$ at 30 $^{o}$C. Samples were collected at the bottom of the column at different time intervals, and then analyzed for pH and metal concentrations using ICP-AES. All experiments were done in triplicates, and the data presented are the average values of three experiments.

### 2.7. Cytotoxicity assay in peripheral blood mononuclear cells

*In vitro* cytotoxicity assay was carried out using the colorimetric MTT assay. Different working stocks of nPMMA samples were prepared, and 0.1 ml of twofold dilution series of nPMMAs was added in a 96-well microtiter plate by using 10% Roswell Park Memorial Institute medium. Stimulated peripheral blood mononuclear cells at $2\times10^5$ per well were added in duplicate to the dilution suspension and the plates incubated for 5 days at 37 °C with humidified 5% $CO_2$ atmosphere. After incubation, cell viability was determined by (4,5-dimethylthiazol-2-yl)-2,5-diphenyltetrazolium bromide assay (Sigma, St. Louis, MO). Then, 20 µl (from a stock of 5 mg $ml^{-1}$) reagent was added in each well and incubated at 37 °C for 4 h in a $CO_2$ incubator. Dimethyl sulfoxide (0.1 ml) was added to each well and kept in the dark for 1 h at room temperature. Optical density was taken at 550 and 630 nm, the latter as a reference wavelength. To determine cell viability, we performed the experiment in triplicate and represented data as mean ± standard deviation. Cell viability (%) of all samples was compared with that of the control (bulk PMMA treated) cells and analyzed using one-way analysis of variance followed by Tukey's least significant difference and Duncan's *post hoc* tests. Statistical analyses were done using MiniTab Ver 16.0 (MiniTab, Inc., State College, PA, USA). Statistical significance was considered at 5% level ($p < 0.05$) along with the control (bulk PMMA).

## 3. Results and discussion

### 3.1. Acoustic atomized microemulsion vs. conventional atomized microemulsion: a comparative account

The particle nucleation and growth mechanism for the polymerization process in this work occurred as follows (Scheme 1). The mechanism included firstly, the formation of three sets of radicals (the $SO_4^{\cdot-}$ radicals generated thermally, the H and OH radicals by the sonolysis of water and the radicals created by the sonochemical degradation of the surfactant and

monomer molecules), their ensuing interaction, reaction and neutralization. The remaining 'useful' radicals then participate in initiation, after which the polymerization proceeds as described elsewhere.[26]

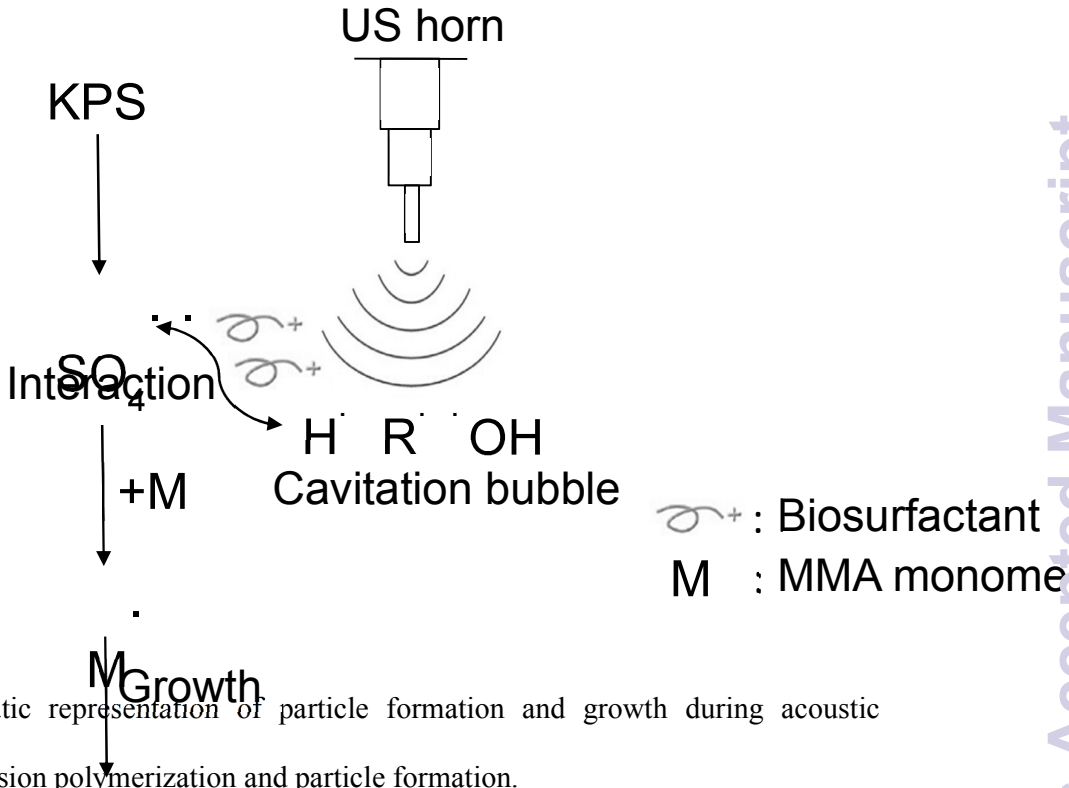


**Scheme 1.** Schematic representation of particle formation and growth during acoustic atomized microemulsion polymerization and particle formation.

As can be seen fr rate of polymerization ( was 91% (rate of polyr ) with particle size of 6 sted method under the ons (i.e., MMA, 5 wt.% MA; surfactin, 0.5% of ; power output, 50% amplitude; time, 1 h). As a comparison, Bhanvase *et al.*[16] reported PMMA of 106 nm in US initiated *in situ* semibatch emulsion polymerization using 4% KPS and 2% SDS. An important appealing feature of our method is the biosurfactant/monomer weight ratio of 0.005, which is much lower than the corresponding amounts reported in the literature.[16,29] In the case of the conventional atomized microemulsion reactions, maximum conversion was 76% (rate of polymerization = 1.26 g $l^{-1}$ $min^{-1}$) and lowest particle size was of 70 nm at optimized conditions (Table 1).

| Product characteristics | $nPMMA_{US}$[a] | $nPMMA_{AM}$[b] |
|---|---|---|
| Monomer conversion, % | 91 | 76 |
| Rate of polymerization, g $l^{-1}$ $min^{-1}$ | 1.51 | 1.26 |
| Solid content (%) | 27.53±0.2 | 25.55±0.2 |
| $t^*_{blue}$ (min)[c] | 04 | 07 |
| Density of core polymer, g $cm^{-3}$[d] | 1.14 | 1.03 |
| Particle size (DLS), nm | 75.5 | 79.5 |
| Particle size (TEM), nm | 60.0 | 70.0 |
| Polydispersity index[e] | 0.56 | 0.61 |
| Total number of latex particles, $N_p \times 10^{18}$ | 7.63 | 6.85 |
| Polymer chains per particle, $N$ | 13 | 16 |
| Percentage of grafted surfactin, $G_{SR}$% | 67 | 31 |
| Shell per core weight ratio, $R_{S:C}$ | 0.21 | 0.09 |
| Amine groups per particle, Am-P ($10^5$) | 46.5 | 22.3 |

[a]Process conditions: MMA, 5 wt.%; KPS, 3% of MMA; surfactin, 0.5% of MMA; temperature, 55 $^oC$; power output, 50% amplitude; time, 1 h.

[b]Process conditions: MMA, 5 wt.%; KPS, 3% of MMA; surfactin, 0.5% of MMA; temperature, 55 $^oC$; agitation, 250 rpm; time, 1 h.

[c]The time when the colour of the microemulsion turns blue.

[d]The parameter was referred to bulk density of the polymer.

**Table 1.** Product characteristics of $nPMMA_{US}$ and $nPMMA_{AM}$.

In addition, US assisted microemulsion polymerization resulted in lower average particle size and narrow particle size distribution. From the size distribution it is also apparent that there are relatively a higher number of larger particles in the atomized microemulsion process compared to the US supported polymerization process. Furthermore, the time required for blue point appearance, an indication of initiation of polymerization and the formation of oligomers,[16] is less in US microemulsion polymerization than atomized microemulsion. It is postulated that increased monomer conversion in acoustic atomized microemulsion could be due to the higher grafting of surfactin and hence, more amount of amine groups in $nPMMA_{US}$. As mentioned earlier that amine groups can form redox pairs with initiator, therefore, the more amine groups led to the more redox pair formation, and the more free radicals. The more amine groups could subsequently enhanced polymerization of the MMA monomer and resulted in higher monomer conversion percentages.

As the mechanism of the polymerization is similar in the case of acoustic atomized microemulsion polymerization (with US horn) and conventional atomized microemulsion (with mechanical stirrer), it was thought desirable to compare the effectiveness of the two modes of emulsion polymerization in terms of the energy efficiency and cavitational yield (see 'Energy calculations' in ESI). The energy utilized for the synthesis of nPMMA has been calculated as the total energy required (kJ) per unit weight of the material (g) present in the system. Total energy required per unit weight of the material present in the acoustic atomized microemulsion polymerization is $9.60 \times 10^{-2}$ kJ $g^{-1}$ and $43.98 \times 10^{-2}$ kJ $g^{-1}$ for the conventional atomized microemulsion method. Thus, acoustic atomized microemulsion polymerization process has proved to be much superior in terms of energy efficiency (saved ~ 96% of energy utilized by the conventional atomized microemulsion). Mirroring this trend, US assisted method gives more than 5 times cavitational yield as compared to the conventional atomized microemulsion, when operated individually under optimum operating conditions for the specific case of emulsion polymerization of MMA (see 'Calculation of cavitational yield' in ESI). It can be clearly seen from the values that the degree of intensification is indeed enhanced due to acoustic cavitation. To date, most of the research work done on acoustic emulsification emphasized on polymerization recipe and effect of US energy. However, this work is the first one to investigate the comparative efficacy of acoustic and conventional atomized microemulsion in terms of energy savings and cavitational yield.

### 3.2. Characterization of $nPMMA_{US}$ and $nPMMA_{AM}$ particles

The nPMMA prepared by both routes (*i.e.* US and conventional atomized microemulsion) shows core/shell morphology. As can be seen from the TEM micrographs, atomized microemulsion resulted in 70 nm particles with uniform size distribution (Fig. 1a); however, core-shell nanostructures are not well-defined. On the other hand, US (at 50% amplitude) gave rise to lowest particle diameter (60 nm) with highly monodisperse core-shell

morphology, (Fig. 1; inset of d), wherein the hydrophobic PMMA cores (darker part) were 55 nm in diameter and coated with biosurfactant shells (light black ring) of 5 nm.

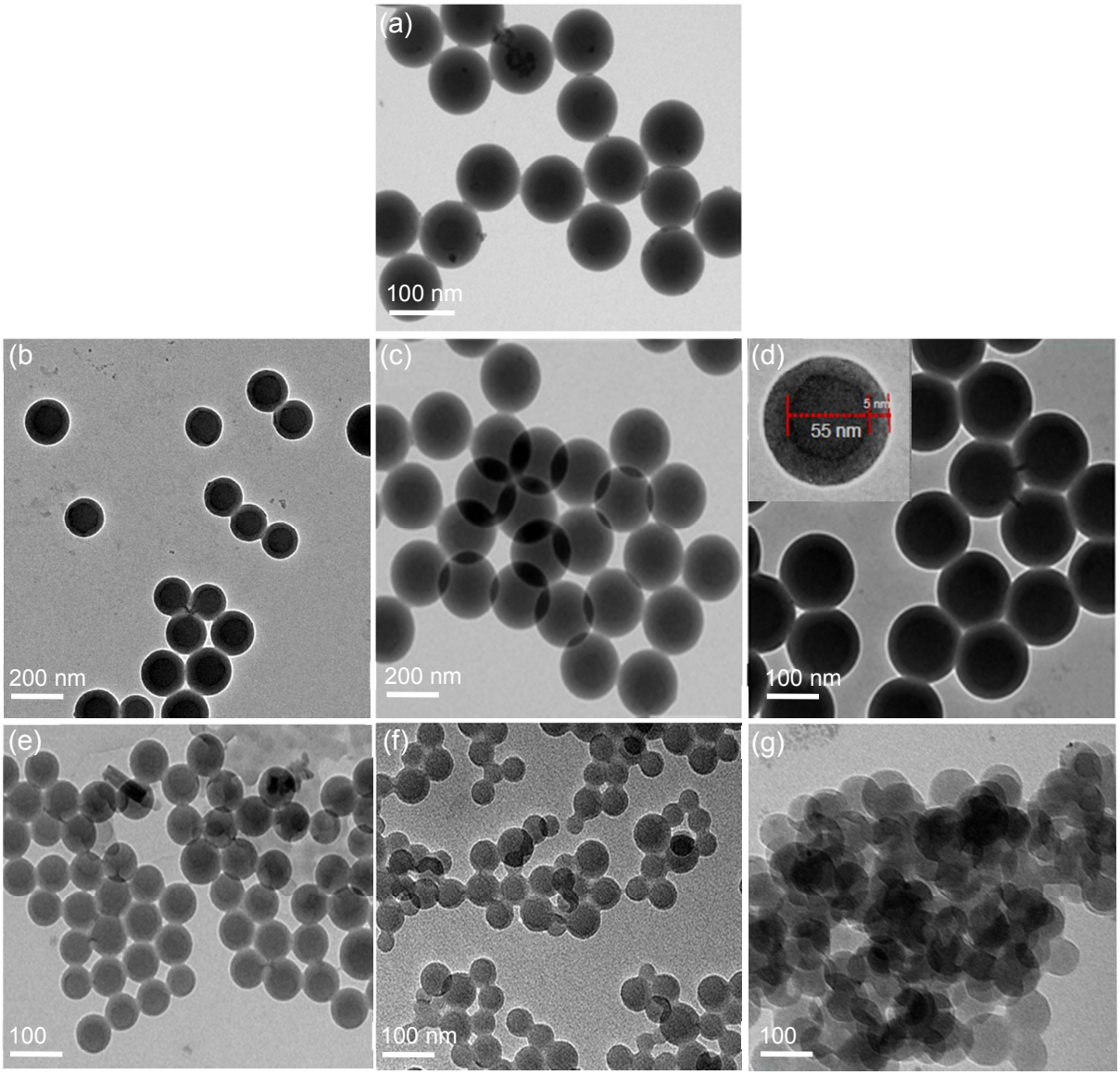


**Fig. 1.** TEM images of (a) $nPMMA_{AM}$ particles. TEM images of $nPMMA_{US}$ particles at acoustic amplitude of (b) 30%; (c) 40%; (d) 50%; (e) 65%; (f) 70%; (g) 80% (process parameters for $nPMMA_{US}$: MMA, 5 wt.%; KPS, 3% of MMA; surfactin, 0.5% of MMA; temperature, 55 $^{o}$C; power output, 50% amplitude; time, 1 h; process parameters for

nPMMA$_{AM}$: MMA, 5 wt.%; KPS, 3% of MMA; surfactin, 0.5% of MMA; temperature, 55 $^{o}$C; agitation, 250 rpm; time, 1 h.).

The surface area of the nanoparticles was calculated using the following expression:[34]

$$N = 6.10^{10}.S/\pi.\rho_s.d^3 \quad (2)$$

where, $N$ is the number of nanoparticles per ml; $S$ is the % of solids; $\rho_s$ is density of the polymer (g ml$^{-1}$); $d$ is the nanoparticle diameter (nm). The number of nanoparticles in ml suspension was determined by utilizing from mass-volume graph. From all these data, specific surface area of the nPMMA$_{US}$ particles was calculated by multiplying $N$ and surface area of 1 nanoparticle. The specific surface area was calculated as 991 m$^2$ g$^{-1}$. Nonetheless, higher US power output led to a more intense mixing environment. This will increase the aggregation of the smaller particles, thus leading to the overall generation of larger particles with a wider distribution (Fig. 1e-g). Here, we show that US assisted atomized microemulsion polymerization was effective to produce relatively smooth surfaced and well-defined core/shell nPMMA with smaller size and narrower distribution.

The effect of pH on particle ζ-potential was investigated at different pH values between 1.0 and 12.0 (Fig. S3; ESI). The surface charges of nPMMA$_{US}$ particles were positive at pH 2-8 due to the protonation of amine groups of surfactin, which strongly revealed that the surface component of nanoparticles was made of surfactin. These nanoparticle dispersions have ζ-potential values higher than +30 mV, and hence, can be described as stable dispersions.[29,35] Also, it is well-documented that the particle number density decreases with increasing particle diameter; hence, the total positive charge provided by the initiator molecule is shared between less numbers of particles for dispersions containing large-diameter particles. This result in a higher surface charge value for larger nanoparticles.[35] Upon increasing solution pH, the ζ-potentials began to decrease confirming

that the isoelectrical point for the latexes coincides with the $pK_a$ of the amine and amidine groups.[36] It even reached to negative values at strong basic pH, resulting from the transformation of protonated amines to neutral ones and then combined with hydroxyl ions. It is noteworthy that highly positive charge can keep the nanoparticles stable in acid and neutral solutions due to the charge repulsion force. Even though the surface charge of $nPMMA_{AM}$ formulation was also positive, it was not high enough as compared to $nPMMA_{US}$ particles. This may be attributed to poor grafting efficiency of surfactin biosurfactant onto PMMA.

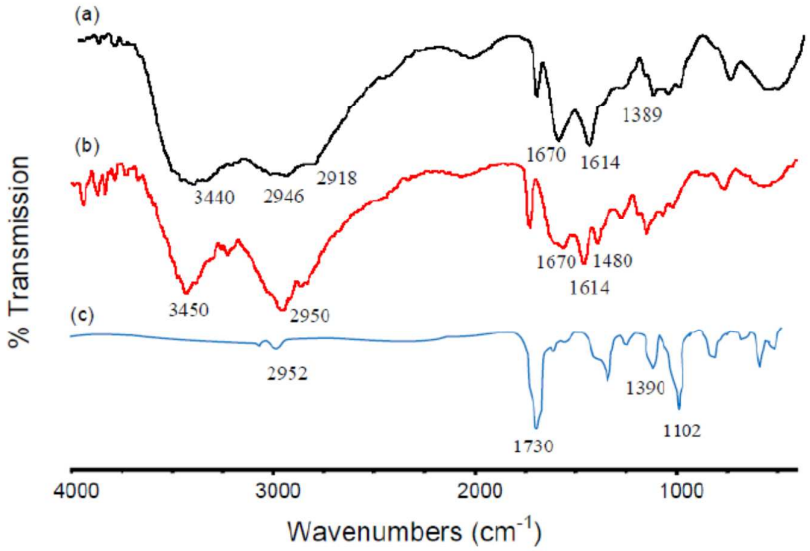


**Fig. 2.** FTIR spectra of (a) pure surfactin, (b) $nPMMA_{US}$ and (c) $nPMMA_{AM}$ particles.

As evident from Fig. 2(a), the wide band around 3440 $cm^{-1}$ could be assigned to the axial stretching vibrations of O-H superimposed to the N-H stretching bands and intermolecular hydrogen bonds. The C-H stretching and bending bands of $-CH_2$ group was observed as a doublet at 2946 and 2918 $cm^{-1}$, respectively.[37] The peaks found at 1670, 1614 and 1389 $cm^{-1}$ are ascribed the C=O of amide I, $-NH_2$ bending of amide II and N-H or C-N stretching of amide III vibrations, respectively.[38] From Fig. 2(b) it is clear that $nPMMA_{US}$ particles display both the characteristic peaks of nPMMA (-C=O at 1730 $cm^{-1}$) and surfactin (N-H stretching at 3450 $cm^{-1}$, asymmetric stretching of $-CH_2$ at 2950 $cm^{-1}$, and $NH_3^+$

vibration at 1670, 1614 $cm^{-1}$ due to amide I, amide II of the -$CO_2NH$- group). There was a new absorption band at 1480 $cm^{-1}$ (*v* -C-O) which shows the presence of -COOH groups in the $nPMMA_{US}$ particles. Fig. 2(c) shows the FTIR spectra of the $nPMMA_{AM}$ polymer. The stretching vibration frequency of (-$CH_3$) appears at wave numbers of 2952 $cm^{-1}$ and the bending vibration frequency of (-$CH_3$) is at a wave number of 1390 $cm^{-1}$. The wave number 1730 $cm^{-1}$ corresponds to the stretching vibration frequency of (-C=O). The wave number 1102 $cm^{-1}$ represents the stretching vibration frequency of (-C-O). These results confirmed that the nanoparticles were consisted of nPMMA and surfactin as a biosurfactant.

To ensure covalent linkage between the biosurfactant shell and the PMMA core, the $nPMMA_{US}$ and $nPMMA_{AM}$ particles were repeatedly washed with water through a centrifugation, decantation, and redispersion cycle until conductivity of the supernatant was equal to that of double distilled and deionized water (DDIW) used, and surfactin in the supernatant was not detectable with the Bradford method. To separate the biosurfactants from the PMMA core, the particles were subjected to acid hydrolysis. The FTIR spectrum of the dried products obtained from after acid hydrolysis was identical to that reported for the PMMA, which further confirmed the formation of nPMMA-biosurfactant core/shell particles. Next, TNBS assay was performed to evaluate the grafting performance, which relates to the attachment of surfactin onto the nanoparticles' surface. It was found that $G_{SR}$ calculated from TNBS assay was 67% and 31% for $nPMMA_{US}$ and $nPMMA_{AM}$ particles, respectively. The lower $G_{SR}$ for $nPMMA_{AM}$ may be mainly contributed by the higher difficulty of hydrophobic monomers to graft from the hydrophilic biosurfactant chains. This may explain why ζ-potential was considerably lower in $nPMMA_{AM}$.

$^1H$ NMR was used to ascertain the molecular structure of PMMA and its surface modification. $^1H$ NMR of $nPMMA_{AM}$ presents peak at 3.8 ppm which represents three protons of $OCH_3$, at 1.8 ppm represents two protons of $CH_2$ and signals appearing at 2.5 ppm

attributed to three protons of $CH_3$ (Fig. 3a). On the other hand, in $nPMMA_{US}$ particles, peak at 3.5 ppm corresponds to 2 protons of $NH_2$ (due to incorporation of surfactin), peak at 3.8 and 4.12 ppm ascribed to two protons of $CH_2$ and peak at 2.0 ppm corresponds to three protons of $CH_3$.[39] The broader peaks labelled around $\delta$ = 8.5 ppm and $\delta$ = 9.0 ppm with roughly Gaussian shapes in the aromatic region of the spectrum confirmed the presence of aromatic amino acids of surfactin (Fig. 3b). Besides, XRD (Fig. S4), DSC (Fig. S5) and TGA (Fig. S6) results showed characteristics of nPMMA particles (see in ESI).

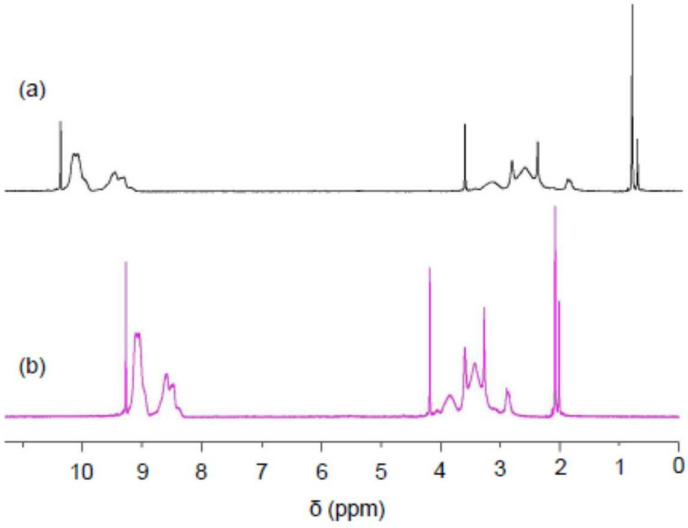


**Fig. 3.** $^1H$ NMR spectrum of (a) $nPMMA_{AM}$ particles and (b) $nPMMA_{US}$ particles.

To further find out the difference in surface chemistry, high energy resolution XPS spectra of the C1s region of $nPMMA_{AM}$ and $nPMMA_{US}$ particles were analyzed in detail. Fig. S7 (in ESI) shows an overlay of the C1s spectra. The C1s spectra that are normalized to the same intensity at energy 284.6 eV can be deconvoluted into 5 different components. One component at 284.6 eV, C1, is assigned to aliphatic carbon, C-C/C-H, which is the major component of pure PMMA, but is also found in low concentrations in spectra from $nPMMA_{US}$ particles (arising from the hydrocarbon of surfactin). The component C2 at 285.2 eV is assigned to β-shifted carbon next to the carbonyl group of PMMA, C-C=O. C3 (286.8

eV) is a convolution of the ether carbon, C-O-C/O-C, found in both PMMA and surfactin and the C-OH carbon of surfactin. The C4 peak at 287.9 eV is O-C-O and C5 (288.8 eV) is from the acrylate bond, O-C=O, of PMMA.[40] The relative concentrations and the atomic concentration (%) of C1, C2, C3, C4 and C5 increased after the chemical modification and surface changes with surfactin (Fig. S7 and Table S2; see ESI). The N 1s signal is not affected by the crosslinking treatment since nitrogen from amino and imino groups exhibit N 1s photoemissions at similar BE's,[40] confirming that the structure is homogeneous in terms of nitrogen sites. The O 1s bands are slightly affected by the chemical modification, as expected by introduction of groups from surfactin. Based on these results, the difference in surface chemistry between $nPMMA_{AM}$ and $nPMMA_{US}$ particles is explained by the better 'covalent immobilization' of the surfactin on the surface of the particles in the latter case.

### 3.3. Adsorption properties of the $nPMMA_{US}$ particles for heavy metal ions

#### 3.3.1. Adsorption kinetics

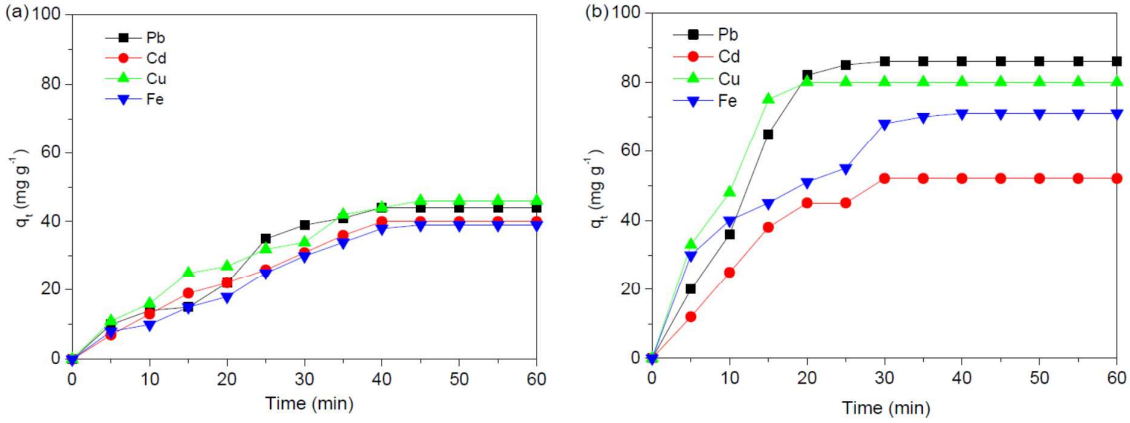


**Fig. 4.** $Pb^{2+}$, $Cd^{2+}$, $Cu^{2+}$ and $Fe^{2+}$ adsorption kinetics on (a) $nPMMA_{AM}$ particles; (b) $nPMMA_{US}$ particles. Values reported as the mean ± S.D. ($n$ = 3).

Maximum adsorption of $Pb^{2+}$, $Cd^{2+}$, $Cu^{2+}$ and $Fe^{2+}$ ions onto the $nPMMA_{AM}$ particles was very low, about 44, 40, 46 and 39 mg $g^{-1}$ after 45 min, respectively (Fig. 4a). The $nPMMA_{AM}$

particles contain few binding sites for complexation of these four metal ions. This very low adsorption may be due to weak interactions between metal ions and hydroxyl groups on the surface of the nPMMA particles; very lower grafting of surfactin onto $nPMMA_{AM}$ have little contribution to the sorption properties. However, incorporation of surfactin as a biosurfactant into the $nPMMA_{US}$ surface significantly increased the adsorption capacity to 86, 52, 80, and 71 mg $g^{-1}$ after 30 min, respectively, for $Pb^{2+}$, $Cd^{2+}$, $Cu^{2+}$ and $Fe^{2+}$ ions. Also with increasing the contact time to 60 min, the adsorption capacity increased. The equilibrium times of different heavy metal ions adsorbed on these nanoparticles were within 60 min. More importantly, more than 65% of heavy metal ions could be removed within 30 min (Fig. 4b). Beyond 30 min, the amount of adsorbed ions remained unchanged. Hence, this duration was chosen as the optimum contact time for all further experiments. The equilibrium time observed here is much less as compared to those reported in earlier works which related with the adsorption of several heavy metal ions on various adsorbents, particularly on poly(hydroxyethyl methacrylate) (PHEMA) and imidazole functionalised PHEMA.[6,34] The high adsorption capacity and fast adsorption equilibrium time achieved with $nPMMA_{US}$ structures may be due to the following: (i) incorporation of surfactin chelating groups into the polymer structure; (ii) long side chain of surfactin acted as a spacer arm that could catch divalent cations easily; and (iii) high complexation rate (i.e., high affinity) between divalent heavy metal ions and amino acids of surfactin in the nanoparticles.

In order to investigate the potential rate controlling step such as the mass transfer or chemical reaction processes, pseudo first-order and pseudo second-order model were tested on these experimental data (details of kinetic models have been explained in ESI). Numerous earlier studies computed the values of $k_1$ and $k_2$ from the plots of ln ($q_e$-$q_t$) vs. t and $t_q/t$ vs. t, respectively.[41-45] However, Low *et al.*[46-48] suggested that the $k_1$ and $k_2$ values should be obtained from the slopes of the plots ln (1- $q_t/q_e$) vs. t for pseudo first-order and $1/q_t$ -$1/q_e$ vs.

1/t for pseudo-second order model, respectively. The obtained experimental data showed that the $R^2$ values for the pseudo-second order model were higher than that of the pseudo first-order model (see Fig. S8 in ESI). Although the $R^2$ values obtained in both models are high, there were appreciable differences between the $q_{t,exp}$ and $q_{t,cal}$ values in pseudo first-order model at the initial stage of adsorption process. The second order rate constant values revealed that this adsorption system followed a better compliance to pseudo second-order model as the values of $q_{t,exp}$ and $q_{t,cal}$ were very close from the initial stage of the adsorption process until the final stage. The results were similar to previous literature reports.[46-48] The adsorption rate constants of $Pb^{2+}$, $Cd^{2+}$, $Cu^{2+}$ and $Fe^{2+}$ calculated based on the pseudo second-order kinetics were $1.22 \pm 0.03 \times 10^{-2}$, $1.37 \pm 0.01 \times 10^{-2}$, $1.35 \pm 0.02 \times 10^{-2}$, and $1.26 \pm 0.05 \times 10^{-2}$ g $(mg.min)^{-1}$. This phenomenon further implies that the dominant mechanism for heavy metal ions sorption on these nanoparticles is chemisorption or strong surface complexation rather than mass transport.[38,39] In previous literature, the pseudo first- and second-order kinetic model was found to be appropriate for describing kinetics of metals[3,5,8,13] and dye[49,50] sorption by different materials. There were two steps for the heavy metal adsorption by $nPMMA_{US}$ particles. In the first 10 min, a large amount of heavy metals were rapidly adsorbed by the exterior surface and amino groups of surfactin in biosurfactant shell. When the adsorption of exterior surface reached saturation, heavy metals entered into the pores and were absorbed by the interior surface of PMMA polymer.

### 3.3.2. Adsorption isotherms

The adsorption isotherm shows how the adsorbate molecules are distributed between the liquid phase and solid phase (details of isotherm models are explained in ESI). It is evident from Fig. 5 and Table 2 that Langmuir isotherm proved to be a better mathematical fit for equilibrium data than Freundlich model (based on the higher $R^2$ value in the linear plots). Moreover, the data for $nPMMA_{US}$ particles fitted better than $nPMMA_{AM}$. In addition, the

values of $n > 1$ indicated favourable adsorption conditions[45,46-48] as observed from Freundlich model for $nPMMA_{US}$ particles. Though the relatively higher $R^2$ values of Langmuir isotherm

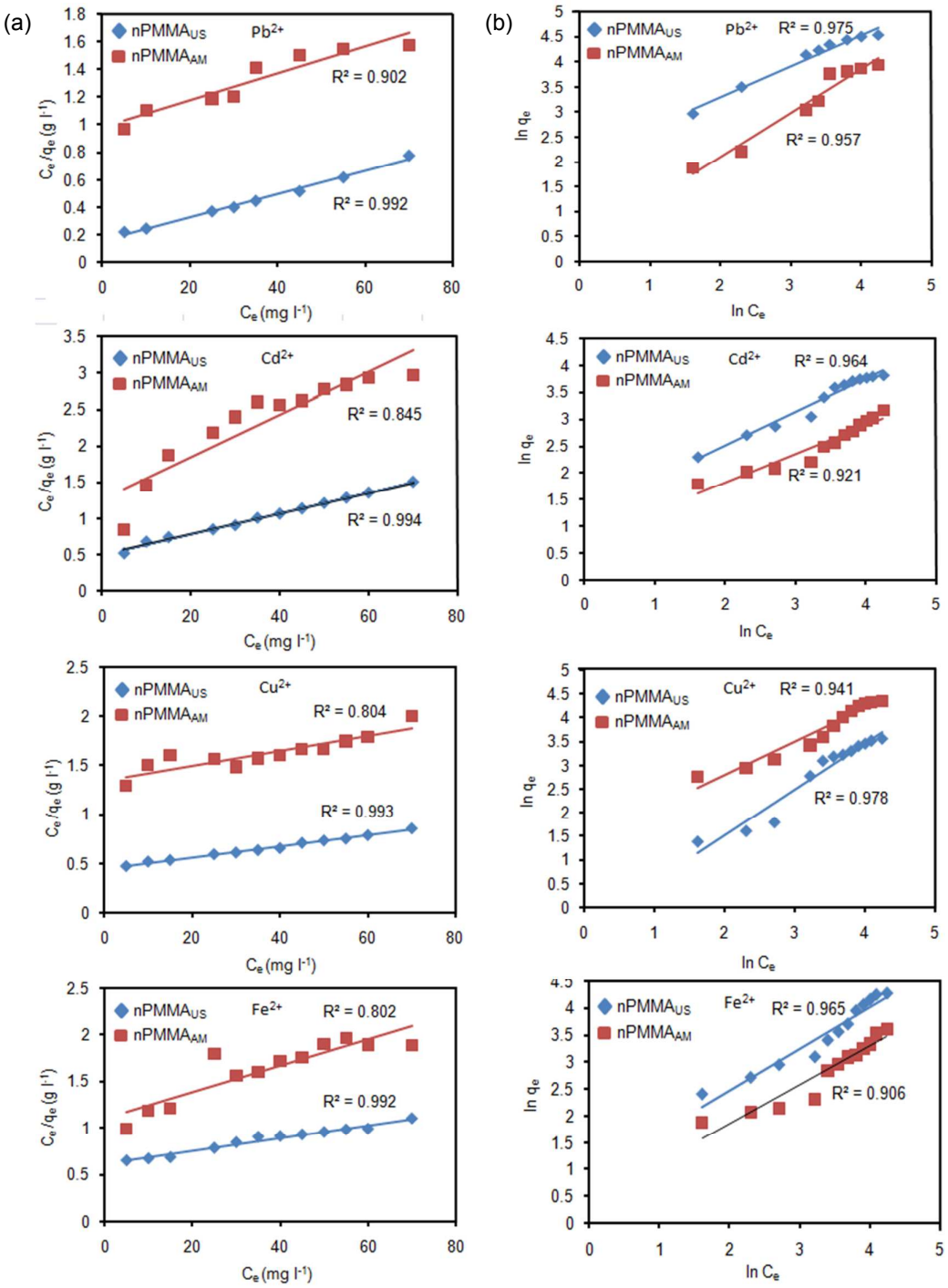

**Fig. 5.** Linear plot of (a) Langmuir and (b) Freundlich adsorption isotherm model (adsorbent loading: 200 mg $l^{-1}$; initial metal ion: 30 mg $l^{-1}$; pH: 6.0; contact time: 30 min). Values reported as the mean ± S.D. ($n$ = 3).

indicated that it is more preferable than Freundlich adsorption, the closeness of these values meant that both of them are almost equally obeyed for $nPMMA_{US}$ particles. It can be concluded that probably the surface of the $nPMMA_{US}$ particles contains heterogenous moieties which are uniformly distributed on the surface which accounts for both Langmuir and Freundlich adsorption isotherms.[46-48,51,52] From the reported literatures,[12-14] it is known that the removal of heavy metal ions is derived from the coordinate interactions and complexation between the metal ions and surface amino groups. Comparing with the maximum adsorption capacity of polymeric adsorbents reported by previous studies,[2,3,5,6-9,12] the prepared $nPMMA_{US}$ particles possessed an absolute advantage with much higher adsorption capacity which may be derived from its larger surface area of the core PMMA polymer and large number of amino acids in the surfactin shell.

| | **Models** | | | | | |
|---|---|---|---|---|---|---|
| **Metal ions** | **Langmuir isotherm** | | | **Freundlich isotherm** | | |
| | $q_{max}$ (mg $g^{-1}$) | $b$ (l $mg^{-1}$) | $R^2$ | $k_f$ | $1/n$ | $R^2$ |
| **$Pb^{2+}$** | 125.70 | 0.039 | 0.992 | 7.95 | 0.61 | 0.975 |
| **$Cd^{2+}$** | 106.50 | 0.043 | 0.994 | 5.88 | 0.52 | 0.964 |
| **$Cu^{2+}$** | 71.13 | 0.049 | 0.993 | 4.96 | 0.48 | 0.978 |
| **$Fe^{2+}$** | 58.76 | 0.056 | 0.992 | 4.25 | 0.44 | 0.965 |

**Table 2.** Isotherm parameters for adsorption of the tested heavy metal ions onto $nPMMA_{US}$ particles.

### 3.3.3. Effect of adsorbent dose

The effect of adsorbent dose on adsorption of $Pb^{2+}$, $Cd^{2+}$, $Cu^{2+}$ and $Fe^{2+}$ was studied using different $nPMMA_{AM}$ and $nPMMA_{US}$ particles dosages in the range of 50-300 mg $l^{-1}$ for 50 mg

$l^{-1}$ of initial metal ion concentration. Fig. S9(a) (see ESI) showed that on increasing adsorbent dose from 50 to 250 mg $l^{-1}$, the adsorption of $Pb^{2+}$, $Cd^{2+}$, $Cu^{2+}$ and $Fe^{2+}$ increased from 44, 20, 16 and 10 mg $g^{-1}$ to 211, 107, 155 and 150 mg $g^{-1}$, respectively. Thereafter, adsorption capacity remained more or less same upto 300 mg $l^{-1}$. On the contrary, $nPMMA_{AM}$ was found to be a poor adsorbent (Fig. S9b in ESI). Such a trend is mainly attributed to an increase in the adsorptive surface area and the availability of more adsorption sites. There was no significant change observed as the adsorbent dose was further increased. This was due to the concentration of metal ions that reached at equilibrium status between solid and solution phase and there is less commensurate increase in adsorption resulting from the lower adsorptive capacity utilization of the adsorbent.[13,14]

It may be argued that the increased adsorption capacity in diluted concentration of nanoparticles is due to the fact that the exposed amine groups on the surfactin shells are easily able to chelate with heavy metal ions and form surface complexes (intra-particle chelation). However, with increasing the concentration of nanoparticles, metal ions can not only be chelated to a single nanoparticle, but also act as bridges to crosslink the surfactin shells of nanoparticles causing formation of aggregates (inter-particle chelation) and numbers of chelating ligands are embedded and blocked. As a consequence, the amount of metal ions adsorbed was decreased in the concentrated solution of $nPMMA_{US}$ nanoparticles. This explanation can be supported by the literature data.[53,54] It seems plausible that square-planar structure was favourable to be induced when heavy metal ions were surrounded with large number of flexible amine groups in the concentrated solution of $nPMMA_{US}$ nanoparticles. Further experimental evidences like electron spin resonance (ESR) method are necessary to validate this hypothesis.[53,54]

### 3.3.4. Effect of initial metal ion concentration

To observe the effect of initial metal ion concentration on adsorption by $nPMMA_{US}$, the experiments were conducted over the range of 5-50 mg $l^{-1}$ for each metal ion. The amount of $Pb^{2+}$, $Cd^{2+}$, $Cu^{2+}$ and $Fe^{2+}$ adsorbed at the equilibrium ($q_e$) increased from 22, 10, 26, 10 mg $g^{-1}$ to 85, 55, 75 and 52 mg $g^{-1}$, respectively, as the concentration was increased from 5 to 30 mg $l^{-1}$ for $Pb^{2+}$, $Cd^{2+}$, $Cu^{2+}$ and $Fe^{2+}$ (Fig. S10a in ESI). However, beyond 30 mg $l^{-1}$, there was no significant change observed in the adsorption capacity. Similar observation was made with the $nPMMA_{AM}$ particles; nevertheless, maximum adsorption was 40 mg $g^{-1}$ with $Fe^{2+}$ at 40 mg $l^{-1}$ (Fig. S10b in ESI). The initial concentration provides an important driving force to overcome all mass transfer resistances of the metal ion between the aqueous and solid phases. Hence a higher initial concentration of metal ion will enhance the adsorption amount of metal ions.

Based on the data obtained from adsorption efficiency and kinetics, $nPMMA_{US}$ particles were chosen for subsequent experiments since its performance was superior as compared to $nPMMA_{AM}$ particles.

### 3.3.5. Effect of pH on adsorption

The pH value is an important determinant in the use of polymers as supports in the metal ion adsorption process. It not only affects the electronic status of the pendant functional groups, for instance protonation/deprotonation of the basic groups or dissociation/association of acidic groups, but it may also alter the oxidation form of the metal ions present in the medium.[2] As expected, the higher the acidic condition, the lower was the adsorption of metal ions (see Fig. S11 in ESI). This may be because of (i) the protonation of the amino groups at the acidic conditions[7] and (ii) competition of $H^+$ and hydronium ions ($H_3O^+$) with metal ions which reduce the adsorption of metal ion.[6] At pH > 4, deprotonation degrees of amine groups were enhanced and their chelating capacities were increased simultaneously which was

consistent with the pH-dependent zeta potential of $nPMMA_{US}$ particles. These polymers had an isoelectric point at pH 8.2 (see Fig. S3 in ESI). With increasing pH, the electrical repulsion force and competition from $H^+$ became weaker, thus the adsorption of heavy metal increased. The observation was consistent with the metal amine complexation-adsorption mechanism, as the amino groups were protonized at low pH, passivating adsorption sites and hence suppressing metal adsorption. Further increase in pH may cause precipitation of metal ions due to formation of hydroxide and the adsorbent was deteriorated with the accumulation of metal ions onto surfaces.[6] Therefore, pH 6.0 was selected as the optimum pH for metal ions adsorption for other studies since at ≥ pH 6, $M(OH)^+$ and $M(OH)_2$ species had significant effect towards the enhancement of metal ions removal.[2,6,9]

### 3.3.6. Effect of humic acid (HA)

Being a natural macromolecular organic matter, HA is ubiquitous in surface and ground water. Amino-functionalized mesoporous silica was shown to be an effective adsorbent for HA removal.[30] For all the four tested heavy metal ions, the adsorption capacity first increased when the HA concentration varied from 0 to 30 mg $l^{-1}$, then decreased (see Fig. S12 in ESI). Adsorption of these heavy metal ions was significantly enhanced after incorporation of HA; a fact that could be explained by formation of complexes with carboxylic and phenolic groups at low concentrations of HA. The results indicated that HA had a significant effect on the adsorption of $Pb^{2+}$, $Cd^{2+}$, $Cu^{2+}$ and $Fe^{2+}$.

### 3.3.7. Effect of background electrolytes/interfering ions

Heavy metal ion pollutants are often presented together with alkaline/earth metal ions in water systems.[2,55] In natural water and wastewater systems, electrolyte cations may compete for the binding sites of sorbents while electrolyte anions may exhibit complexation toward metal ions, both of which would greatly influence the sorption process. Fig. S13 (see in ESI)

demonstrates the sorption of $Pb^{2+}$, $Cd^{2+}$, $Cu^{2+}$ and $Fe^{2+}$ as a function of coexisting $Na^{+}$, $K^{+}$, or $Mg^{2+}$. Although the adsorption capacity significantly decreased with increasing coexisting ions in the region of 0-0.05 mol $l^{-1}$, the adsorption capacity slightly decreased with ≥ 0.05 mol $l^{-1}$ coexisting ions; especially, the plateau in the adsorption capacity reached at 0.1 mol $l^{-1}$. The divalent ion, $Na^{2+}$, had an obvious suppressive or competition effect on all these ions adsorption, providing further evidence that the removal is dominated by inner-sphere surface complexation.

### 3.3.8. Adsorption thermodynamics

To study the effect of temperature on the adsorption of metal ions on $nPMMA_{US}$, experiments were conducted at three different temperatures 303, 313 and 323 K. It was observed that the adsorption decreased with increasing temperature, which indicated a low temperature favours metal ion removal by adsorption onto these nanoparticles. This is reasoned from the tendency of metal ions to escape from the solid phase to the bulk phase with an increase in temperature of the solution. A similar observation was also reported on uptake of Ni(II), Co(II) and Cu(II) onto poly[N-(4-[4-(aminophenyl)methylphenylmethacrylamide])].[39]

Thermodynamic parameters such as enthalpy ($\Delta H^o$), entropy ($\Delta S^o$) and Gibb's free energy ($\Delta G^o$) are described in ESI. The values of $\Delta H^o$ and $\Delta S^o$ were determined from the slope ($-\Delta H^o/R$) and the intercept ($-\Delta S^o/R$) of the plots of ln ($q_e m$ / $C_e$) vs. 1/T (see Fig. S13 in ESI).

| Metal ions | $\Delta H^o$ (kJ $mol^{-1}$) | $\Delta S^o$ (J $mol^{-1}K^{-1}$) | $\Delta G^o$ (kJ $mol^{-1}$) | | |
|---|---|---|---|---|---|
| | | | 303 K | 313 K | 323 K |
| $Pb^{2+}$ | -18.415 | -48.08 | -3.847 | -3.366 | -2.886 |
| $Cd^{2+}$ | -9.403 | -30.58 | -0.136 | 0.168 | 0.474 |
| $Cu^{2+}$ | -11.481 | -39.47 | 0.479 | 0.873 | 1.254 |
| $Fe^{2+}$ | -12.455 | -40.44 | 0.475 | 0.867 | 1.233 |

**Table 3.** Thermodynamic parameters of $Pb^{2+}$, $Cu^{2+}$, $Cd^{2+}$ and $Fe^{2+}$ ions adsorption onto surfaces of $nPMMA_{US}$ particles.

The values of thermodynamic parameters are presented in Table 3. Negative $\Delta H^o$ suggested the adsorption process was exothermic in nature. Negative values of $\Delta G^o$ for the adsorption at all three temperatures indicated that the adsorption process was feasible and spontaneous in nature. On the contrary, a positive value of $\Delta G^o$ suggests that (i) desorption is more dominant than adsorption; (ii) the matrix or the polymer in question has lower affinity toward the target metal ion; and (iii) possibly the adsorption process is not spontaneous or energetically favourable.[39] Negative value of $\Delta S^o$ described the decrease in randomness at the adsorbent-solution interface during the adsorption. The results are similar to previous literatures.[6,7]

### 3.4. Desorption and repeated use

For practical application and from the economics standpoint, the recycling and regeneration of the adsorbent is indispensable. To evaluate the possibility of regeneration and reuse of the $nPMMA_{US}$, adsorption-desorption studies were carried out. It was observed that the adsorption capacity was constant and no difference in desorption capacity was observed during the first five sorption-desorption cycles (see Fig. S15 in ESI). Since 0.01 mol $l^{-1}$ HCl or EDTA solutions were used as the desorbing agents and the nanoparticles were vaccum dried at 40 $^oC$ during regeneration, each adsorption-desorption process must experience an HCl or EDTA treatment and a heat treatment. Thus, the reproducibility of these nanopartilces also showed its good stability. These results are in agreement with the reported studies on the reuse of amino-functionalized polymeric materials.[34,55]

### 3.5. Continuous filtering adsorption of heavy metal ions

In the contemporary water purification process, removing heavy metal ions from water with low pollutant concentration is a challenge task for adsorbent materials. Moreover, removing heavy metal ions via continuous filtering adsorption by high performance nanostructures has rarely been reported in the literature. Therefore, a continuous filtering adsorption device for the adsorption of heavy metal ions was designed to remove metal ions and the schematic diagram is shown in Fig. 6(a). Fig. 6(b) shows the concentration of residual heavy metal ions in heavy metal ion aqueous solutions with an initial concentration of 30 mg $l^{-1}$ as a function of the treated capacity of $nPMMA_{US}$ particles after being continuously treated. Considering the maximum permissible discharge limits of heavy metal ions for drinking water set by the World Health Organization and US EPA, *i.e.,* 0.006 mg $l^{-1}$ for $Pb^{2+}$, 0.01 mg $l^{-1}$ for $Cd^{2+}$, 0.25 mg $l^{-1}$ for $Cu^{2+}$ and 0.1 mg $l^{-1}$ for $Fe^{2+}$, the treatment capacity of the studied particles for heavy metal ions is 3.5 g $g^{-1}$ for $Pb^{2+}$, 7.0 g $g^{-1}$ for $Cd^{2+}$, 13.0 g $g^{-1}$ for $Cu^{2+}$ and14.0 g $g^{-1}$ for $Fe^{2+}$ (Fig. 6b). This result suggests that $nPMMA_{US}$ particles have a quite good removal capacity for low concentration heavy metal ions, and that the continuous filtering adsorption method is practical for water treatment.

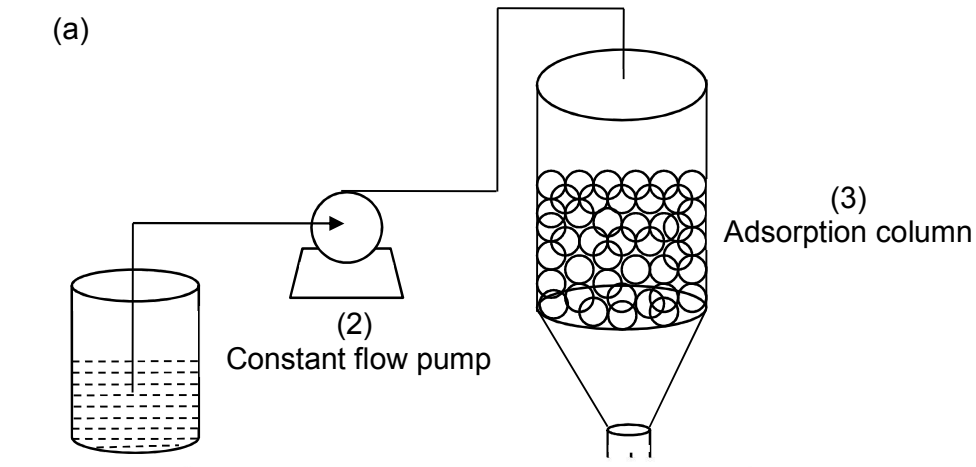

**Fig. 6.** (a) Schematic diagram of continuous column filtering adsorption of heavy metal ions on $nPMMA_{US}$ particles and (b) treatment capacity of $nPMMA_{US}$ particles on metal aqueous solutions with an initial concentration of 30 mg $l^{-1}$.

### 3.6. Adsorption mechanism

To elucidate the reaction mechanisms occurring on the nanoadsorbents, FTIR spectra of the $nPMMA_{US}$ before and after metal adsorption are shown in Fig. 7.

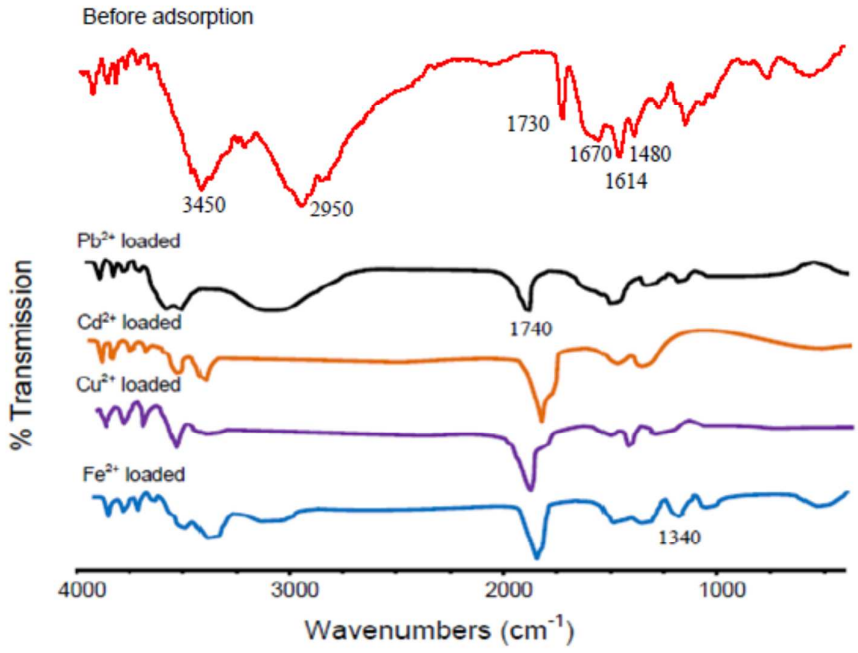


**Fig. 7.** FTIR spectra of $nPMMA_{US}$ particles before and after adsorption.

Before adsorption, two absorption bands at 1730 and 1480 $cm^{-1}$ correspond to stretching vibration of -C=O and *v*-C-O of -COOH groups, a typical characteristic of nPMMA. Also, it

shows N-H stretching at 3450 $cm^{-1}$, asymmetric stretching of -$CH_2$ at 2950 $cm^{-1}$, and $NH_3^+$ vibration at 1670, 1614 $cm^{-1}$ due to amide I, amide II of the -$CO_2$NH- group present in surfactin. The peak at 3450 $cm^{-1}$ turned to a shoulder and also exhibit shifts to different extents after contact with $Pb^{2+}$, $Cu^{2+}$, $Cd^{2+}$ and $Fe^{2+}$ adsorption, and this may indicate a strong metal ions interaction with N-H of amides. Similarly, $NH_3^+$ vibration of amide I, amide II bands at 1670 and 1614 $cm^{-1}$ was of much lower intense and broader after contact with metal ions. Thus, it seems plausible that amide groups of amino acids present in surfactin (shell) definitely play a role in adsorption of these heavy metal ions. Moreover, bands at 1730 and 1480 $cm^{-1}$ also experience shifts to different extents after treatment with metal ions. This suggests that the deprotonated carboxyl forms (carboxylate anions) on nPMMA (core) interacted with metal ions. The peak at 1340 $cm^{-1}$ (ascribed to C-O stretch of COO-M groups) indicates the presence of metal-carboxylate complex.[56] The difference ($\Delta v$) between $v_{asym}$ ($COO^-$) and $v_{sym}$ ($COO^-$) in the wave number region of 1300-1750 $cm^{-1}$ is larger than 200 $cm^{-1}$ in this study, suggesting the formation of metal-carboxylate complex through unidentate chelating coordination.[56] This is further supported by the TEM image of adsorbed $Pb^{2+}$, $Cu^{2+}$, $Cd^{2+}$ and $Fe^{2+}$ ions onto $nPMMA_{US}$ particles (Fig. 8) which shows surface complexes between these metal ions and the chelating ligands of the nanoparticles.

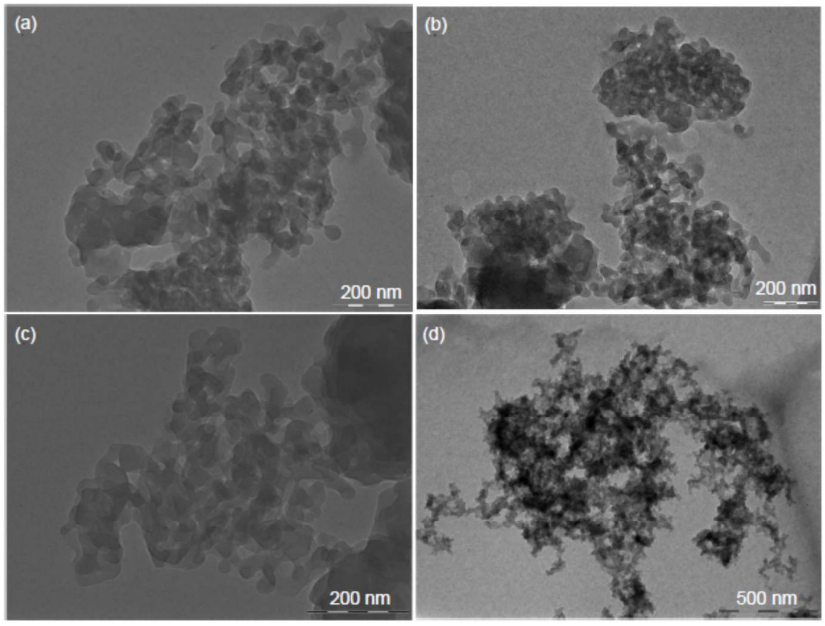


**Fig. 8.** TEM images of $nPMMA_{US}$ particles after adsorption of (a) $Pb^{2+}$, (b) $Cd^{2+}$, (c) $Cu^{2+}$ and (d) $Fe^{2+}$.

A decrease in the atomic concentration for C 1s from XPS data was observed for metals complexed $nPMMA_{US}$ particles, compared to the material before metals adsorption (Fig. S7 and Table S2 in ESI). It indicates that metals adsorption can take place on the structure resulting from primary amino and aldehyde terminal (imino bound), not discarding the possibility of interaction with hydroxyl and non-reacted amino groups that are also present in $nPMMA_{US}$ particle matrices.[57,58] However, a slight increase in the percent contribution of β-shifted C is observed; this increase can be explained by the oxidation of metal on the surface. There is a definite decrease of the percent contribution of C-$NH_2$, but like in the analysis of carbon spectra, the decrease is smaller. This indicates probably a simultaneous protonation of amino groups and formation of complex compounds on non-protonated amino groups. However, it seems that the protonation is a faster reaction, which as a consequence, causes non-reactivity of the $NH_2$ groups. It is also probable to explain the unavailability of certain part of amino groups connected with polymer crystallinity.[58] Therefore, this study allows us

to conclude that the amide groups of surfactin (shell) form coordination bonds with $M^{2+}$ through carbonyl bond (Scheme 2a). Carboxylic groups of nPMMA (core) interact with $M^{2+}$ through the formation of square planner complex[59] (Scheme 2b).

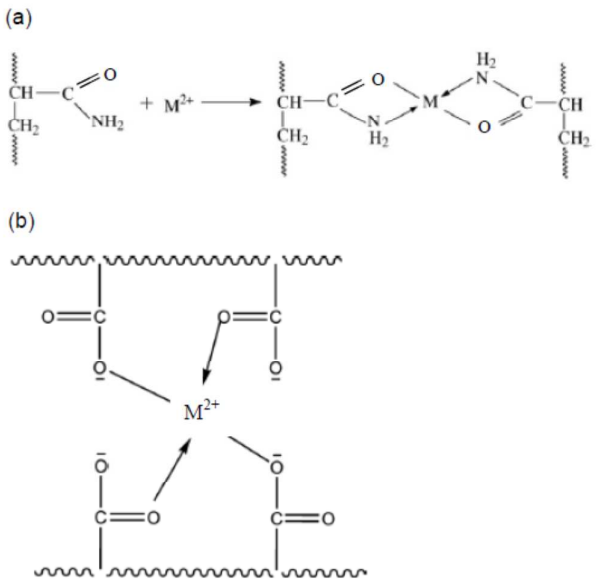


**Scheme 2.** Proposed schematic illustration of the complex formation between metal ions and $nPMMA_{US}$ particles by (a) amide groups of surfactin (shell) through nitrogen and oxygen atoms of carbonyl group and (b) square planner complex between carboxylic groups of nPMMA (core) with heavy metals.

### 3.7. Cellular cytotoxicity assessment

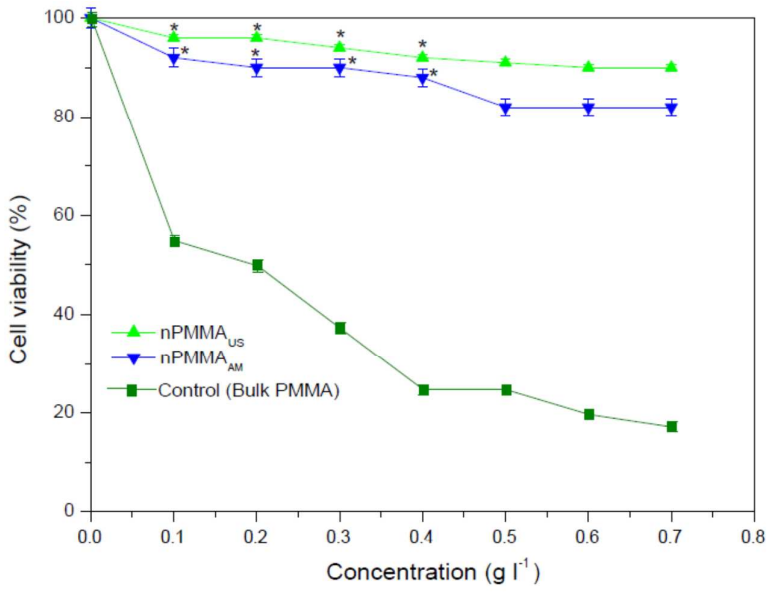


**Fig. 9.** (a) Cytotoxicity of $nPMMA_{US}$ and $nPMMA_{AM}$ against human peripheral blood mononuclear cells. Data represented are mean ± S.D. (standard deviation) of triplicate. *Statistically significant difference as compared to the control ($p < 0.05$ for each).

It is significant to study the biocompatibility behaviour of PMMA because unwanted biological effects induced by the suppression of the phagocytic and antibacterial activity of human polymorphonuclear leukocytes is claimed to be a serious health concern due to PMMA particulate carrier toxicity. Hence, the cytotoxicity of the nPMMA coated with biosurfactants on human peripheral blood mononuclear cells was investigated. It was observed that as the concentration of the nanoparticles increased, the cell survival rate significantly decreased with $nPMMA_{US}$ and $nPMMA_{AM}$ treatment (Fig. 9). This is particularly true in the range of 0.1-0.4 g $l^{-1}$ ($p < 0.05$ for each). However, higher concentrations (0.5 to 0.7 g $l^{-1}$) did not produce significant cytotoxicity to cells ($p > 0.05$ for each). Nonetheless, $nPMMA_{US}$ was more biocompatible as compared to $nPMMA_{AM}$. Considering the amphiphilic nature of surfactin and the bioinertness of MMA, the material was supposed to be biocompatible. Our data showed an excellent non-toxicity profile of $nPMMA_{US}$ even up to 0.7 g $ml^{-1}$. It has been well known that a major problem limiting the

use of amine-containing polymers in biomedical applications is its high cytotoxicity caused by its cationic characteristics.[60] Besides, a clear toxicity related to SDS was observed in nPMMA on 4T1 murine cell line by Colombo *et al.*[61] Thus, it may be implied that $nPMMA_{US}$ could be the candidate for intracellular carriers in biomedical applications such as gene, protein, and drug delivery systems.

### 3.8. Comparison with other polymeric adsorbents

With illustrative purposes, the adsorption capacity of $nPMMA_{US}$ particles for $Pb^{2+}$, $Cd^{2+}$, $Cu^{2+}$ and $Fe^{2+}$ ions was compared with that of other adsorbents reported in the literature and are summarized in Table S3 (see in ESI). It can be found that the adsorption capacities of $nPMMA_{US}$ are higher than some reported hydrogels, for example, methacryloylamidoglutamic acid incorporated porous poly(methyl methacrylate) beads, poly(hydroxyethyl methacrylate/maleamic acid), poly(acrylamide-co-sodium methacrylate), poly(guanidine modified 2-acrylamido-2-methylpropan sulfonic acid/acrylic acid/N-vinylpyrrolidone/2-hydroxyethyl methacrylate) and chitosan. Hence, it can be concluded that the adsorbent synthesized in this study has obvious comparative and competitive advantages. The results are of greater environmental concern as it signifies that these nanoparticles have certain application prospect in metal uptake.

## 4. Conclusions

There is a promising scope for the development of advanced adsorbents with high selectivity, and enhanced separation capacity in environmental application. Taking the principle of acoustic cavitation step further, we have reported a green, one-step, chemical surfactant-free system, in which the combined use of a biosurfactant (at biosurfactant/monomer weight ratio of 0.005, which is much lower than the corresponding amounts reported in the literature) and US improves monomer conversion, particle size and hitherto unreported highly monodisperse

nPMMA (core)-biosurfactant (shell) particles with higher grafting efficiency. It also significantly intensifies the process with overall reduction in the energy requirements and increased cavitational yield. This study demonstrated that $nPMMA_{US}$ core/shell particles could be used as an effective adsorbent for the treatment of heavy metals contaminated wastewater. The adsorption process, which was achieved through the complexation of metal ions by amino groups, is dependent on several factors such as contact time, adsorbent dose, equilibrium metal ions concentration, medium pH, coexisting organic matter (humic acid) and interfering background ions. Adsorption reaches equilibrium within 30 min and the kinetics of $Pb^{2+}$, $Cd^{2+}$, $Cu^{2+}$ and $Fe^{2+}$ adsorption follows the pseudo-second-order model. The maximum uptake capacities for $Pb^{2+}$, $Cd^{2+}$, $Cu^{2+}$ and $Fe^{2+}$ were 86, 52, 80, and 71 mg $g^{-1}$, respectively at 30 $^{o}$C and the equilibrium data are fitted well by the Langmuir model. In multi-metal solutions, these nanoparticles could remove target metal ions with the selectivity order of $Pb^{2+} > Cu^{2+} > Cd^{2+} > Fe^{2+}$. Thermodynamic parameters revealed that the adsorption process was favoured at lower temperature, thermodynamically feasible, spontaneous and exothermic. The heavy metals loaded on these nanoparticles could be desorbed in acid or EDTA solution and adsorption capacity of the regenerated adsorbent was not significantly declined after five cycles of adsorption-desorption cycles. Our results suggest that $nPMMA_{US}$ core/shell particles can be used as a cost-effective reusable absorbent for easy, convenient, and efficient removal of heavy metal ions from wastewater as well as continuous filtering for drinking-water purification.

**Acknowledgements**

This work was financially supported by University Grants Commission (U.G.C), New Delhi [F.No.41-375/2012 (SR), dated July 16, 2012]. Department of Science and Technology (D.S.T), New Delhi and Council for Scientific and Industrial Research (C.S.I.R), New Delhi

are earnestly acknowledged for providing INSPIRE-SRF and CSIR-SRF to Chinmay Hazra and Debasree Kundu, respectively.

## References


1 M. Shahadat, S.A. Nabi, R. Bushra, A.S. Raeissi, K. Umar, M.O. Ansari, *RSC Advances*, 2012, **2**, 7207-7220.

2 K. Tekin, L. Uzun, C.A. Sahin, S. Bektas, A. Denizli, *React. Funct. Polym.* 2011, **71**, 985-993.

3 E.S. Abdel-Halim, S.S. Al-Deyab, *React. Funct. Polym.* 2014, **75**, 1-8.

4 S. Jana, A. Saikia, M.K. Purkait, K. Mohanty, *Chem. Eng. J.* 2011, **170**, 209-219.

5 S. Emik, *React. Funct. Polym.* 2013, **75**, 63-74.

6 O. Moradi, M. Aghaie, K. Zare, M. Monajjemi, H. Aghaie, *J. Hazard. Mater.* 2009, **170**, 673-679.

7 J. Aguado, J.M. Arsuaga, A. Arencibia, M. Lindo, V. Gascón, *J. Hazard. Mater.* 2009, **163**, 213-221.

8 S. Saber-Samandari, S. Saber-Samandari, M. Gazi, *React. Funct. Polym.* 2013, **73**, 1523-1530.

9 Q. Yuan, N. Li, Y. Chi, W. Geng, W. Yan, Y. Zhao, X. Li, B. Dong, *J. Hazard. Mater.* 2013, **254-255**, 157-165.

10 M. Bhaumik, A.Maity, V.V. Srinivasu, M.S. Onyango, *Chem. Engg. J.* 2012, **181-182**, 323-333.

11 N. Wu, H. Wei, L. Zhang, *Environ. Sci. Technol.* 2012, **46**, 419-425.

12 L. Uzun, D. Turkmen, E. Yılmaz, S. Bektas, A. Denizli, *Colloids Surf. A* 2008, **330**, 161-167.

13 F. Fu, Q. Wang, *J. Environ. Manage.* 2011, **92**, 407-418.

14 B. Pan, B. Pan, W. Zhang, L. Lv, Q. Zhang, S. Zheng, *Chem. Engg. J.* 2009, **151**, 19-29.

15 D. Arunbabu, T. Jana, *J. Colloid Interface Sci.* 2011, **361**, 534-542.

16 B.A. Bhanvase, D.V. Pinjari, S.H. Sonawane, P.R. Gogate, A.B. Pandit, *Ultrason. Sonochem.* 2012, **19**, 97-103.

17 S. Mishra, A. Chatterjee, *Polym. Plast. Tech. Engg.* 2010, **49**, 791-795.

18 S. Mishra, A. Chatterjee, *Polym. Adv. Tech.* 2011, **22**, 1547-1554.

19 S. Mishra, A. Chatterjee, V.K. Rana, *Polym. Adv. Tech.* 2011, **22**, 1802-1811.

20 S. Mishra, A. Chatterjee, *Polym. Adv. Tech.* 2011, **22**, 1593-1601.

21 A. Chatterjee, S. Mishra, *Macromol. Res.* 2012, **20**, 780-788.

22 C. Hazra, D. Arunbabu, D. Kundu, A. Chaudhari, T. Jana, *J. Chem. Technol. Biotechnol.* 2013, **88**, 1551-1560.

23 C. Hazra, D. Kundu, A. Chatterjee, A. Chaudhari, S. Mishra, *Colloid Surf. A* 2014, **49**, 96-114.

24 M. Bradley, F. Grieser, *J. Colloid Interface Sci.* 2002, **251**, 78-84.

25 B.M. Teo, S.W. Prescott, M. Ashokkumar, F. Grieser, *Ultrason. Sonochem.* 2008, **15**, 89-94.

26 K. Prasad, S. Sonawane, M. Zhou, M. Ashokkumar, *Chem. Engg. J.* 2013, **219**, 254-261.

27 C.G. Dobie, K.V.K. Boodhoo, *Chem. Eng. Proc. Process Intensif.* 2010, **49**, 901-911.

28 I. Korkut, M. Bayramoglu, *Ultrason. Sonochem.* DOI: 10.1016/j.ultsonch.2013.12.028.

29 W. Chen, X. Liu, Y. Liu, Y. Bang, H.-I. Kim, *Colloids Surf. A* 2010, **364**, 145-150.

30 Y.L. Tang, S. Liang, S.L. Yu, N.Y. Gao, J. Zhang, H.C. Guo *et al.*, *Colloids Surf. A* 2012, **406**, 61-67.

31 X.Y. Liu, H. Namir, S.Z. Yang, B.Z. Mu, *Prot. Pept. Lett.* 2007, **14**, 766-773.

32 H. Namir, X.Y. Liu, S.Z. Yang, B.Z. Mu, *Prot. Pept. Lett.* 2008, **15**, 265-269.

33 S. Mishra, A. Chatterjee, Indian Patent Application No. 254969, 10/01/2013.

34 D. Türkmen, E.Yılmaz, N. Öztürk, S. Akgöl, A. Denizli, *Mater. Sci. Engg. C* 2009, **29**, 2072-2078.

35 S.T. Camli, F. Buyukserin, O. Balci, G.G. Budak, *J. Colloid Interface Sci.* 2010, **344**, 528-532.

36 A.M. Santos, A.Elaı¨ssari, J.M.G. Martinho, C. Pichot, *Polymer* 2005, **46**, 1181-1188.

37 T.S. Anirudhan, S. Rijith, *J. Environ. Radioactivity* 2012, **106**, 8-19.

38 Z. Li, Y. Wang, N. Wu, Q. Chen, K. Wu, *Environ. Sci. Pollut. Res.* 2013, **20**, 1511-1525.

39 A.K. Kushwaha, N. Gupta, M.C. Chattopadhyay, *Arabian J. Chem.* DOI: 10.1016/j.arabjc.2013.06.007.

40 T. Uyar, R. Havelund, Y.Nurd, A. Baland, J. Hacaloglud, L. Toppared, F. Besenbacher, P. Kingshott, *J. Mem. Sci.* 2010, **365**, 409-417.

41 I.D. Mall, V.C. Srivastava, N.K. Agarwal, *Dyes and Pigments* 2006, **69**, 210-223.

42 V.S. Mane, I.D. Mall, V.C. Srivastava, *Dyes and Pigments* 2007, **73**, 269-278.

43 I.A.W. Tan, B.H. Hameed, A.L. Ahmad, *Chem. Eng. J.* 2007, **127**, 111-119.

44 B.H. Hameed, *J. Hazard. Mater.* 2009, **162**, 344-350.

45 B.H. Hameed, D.K. Mahmoud, A.L. Ahmad, *J. Hazard. Mater.* 2008, **158**, 499-506.

46 L.W. Low, T.T. Teng, A. Ahmad, N. Morad, Y.S. Wong, *Water Air Soil Pollut.* 2011a, **218(1-4)**, 293-306.

47 L.W. Low, T.T. Teng, A.F.M. Alkarkhi, A. Ahmad, N. Morad, *Water Air Soil Pollut.* 2011b, **214(1-4)**, 185-195.

48 C. X.-H. Su, T.T. Teng, A.F.M. Alkarkhi, L.W. Low, *Water Air Soil Pollut.* 2014, **225**, 1941-1952.

49 S.R. Shirsath, D.V. Pinjari, P.R. Gogate, S.H. Sonawane, A.B. Pandit, *Ultrason. Sonochem.* 2013, **20**, 277-286.

50 S.R. Shirsath, A.P. Patil, R. Patil, J.B. Naik, P.R. Gogate, S.H. Sonawane, *Ultrason. Sonochem.* 2013, **20**, 914-923.

51 L.W. Low, T.T. Teng, A.F.M. Alkarkhi, N. Morad, B. Azahari, *Sep. Sci. Technol.* 2014, **49(7)**, 1104-1118.

52 L.W. Low, T.T. Teng, Mohd. Rafatullah, N. Morad, B. Azahari, *Sep. Sci. Technol.* 2013, **48(11)**, 1688-1698.

53 A. Wu, J. Jia, S. Luan, *Colloids Surf. A* 2011, **384**, 180-185.

54 L.S. Molochnikov, E.G. Kovalyova, A.A. Zagorodni, M. Muhammed, Y.M. Sultanov, A.A. Efendiev, *Polymer* 2003, **44**, 4805-4815.

55 J. Wang, S. Zheng, Y. Shao, J. Liu, *J. Colloid Interface Sci.* 2010, **349**, 293-299.

56 A. Kurniawan, A.N. Kosasih, J. Febrianto, Y.H. Ju, J. Sunarso, N. Indraswati, S. Ismadji, *Chem. Engg. J.* 2011, **172**, 158-166.

57 R.S. Vieira, M.L.M. Oliveira, E. Guibal, E. Rodríguez-Castellón, M.M. Beppu, *Colloids Surf. A* 2011, **374**, 108-114.

58 Z. Modrzejewska, *React. Funct. Polym.* 2013, **73**, 719-729.

59 M.M. Sinna, T. Siyam, S. Mahdy, *J. Macromol. Sci. A Pure Appl. Chem.* 2004, **A41**, 1187-1203.

60 M. Ratanajanchai, S. Soodvilai, N. Pimpha, P. Sunintaboon, *Materials Sci. Eng. C* 2014, **34**, 377-383.

61 C. Colombo, M. Lupi, P. Ubezio, D. Moscatelli, *Macromol. Symp.* 2013, **324**, 134-139.